LA-UR-04-5865

A Shape Descriptor Based on the Line Scan Transform

Michael Cannon and Tony Warnock

Abstract - We present a shape descriptor that uniquely describes an object, is supported in *n*-dimensional space, and is statistical in nature. The descriptor is based on the line scan transform of Cabo and Baddeley. We show several applications of the descriptor.

Index Terms – shape, shape descriptor, shape metric.

1 Introduction

Shape description is an important part of machine learning and scientific data analysis. A shape description method results in a shape descriptor which can be compared to other descriptors in order to categorize and/or better understand the object under study. Pavlidis [1] divides shape description methods into two categories, those based on shape boundary points and those based on the interior of the shape. If boundary points are used, the shape descriptor can be represented by its Fourier transform [2], a chain code [3], or its bending energy [4]. If the interior of the shape is used, then the shape descriptor might be represented by the medial axis [5], moments [6], or mathematical morphology [7]. Sensitivity to noise and small shape variations are two important considerations when selecting a descriptor, as is the ability to uniquely reconstruct the shape from its descriptor. Objects are compared by comparing their descriptors, which are conceptually subtracted from each other to form a scalar metric – the closer the shape of the objects, the smaller the difference in metric value.

The shape descriptor described in this paper is based on the line scan transformation of Cabo and Baddeley [8]. It has the nice feature of taking both boundary points *and* shape interior into consideration and, unlike most descriptors, it uniquely represents the shape of an object or set of objects when a sufficiently large sample of lines is used. It is supported in *n*-dimensional space and is also statistical in nature in that it is based on a random sampling process, and in this regard it is similar to work by Osada [9] on length distributions in which shapes are compared by comparing histograms of line lengths.

2 Descriptor Components

The shape descriptor described in this paper is composed of a sum of line scan transforms; each transform is computed on a line randomly thrown across an object or set of objects. The metric is the absolute difference between the descriptors of two sets.

2.1 The Line Scan Transform

Our description of the line scan transform in Euclidean space $\Re^d$ is based on the work of Cabo and Baddeley [10] . A set of objects, $S \subset \Re^d$, is defined as a collection of any number of convex and concave objects as shown in the two-dimensional example in Figure 1.

• Both authors are with Los Alamos National Laboratory, Los Alamos, NM 87545. E-mail tmc@lanl.gov and ttw@lanl.gov.

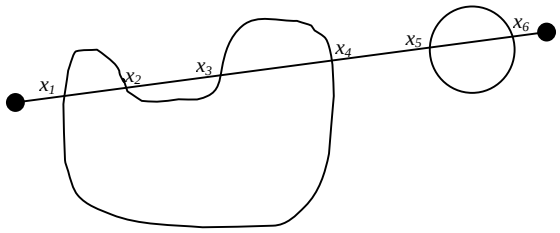

Figure 1. A set of objects in $\Re^2$ intersected with a line to form a set of closed intervals.

The intersection $l \cap S$ of a line l with the set is a finite union of n compact intervals with ordered endpoints $x_1, x_2, x_3, ...x_{2n}$. In the case of our example, the intervals are $x_2 - x_1$, $x_3 - x_2$, $x_4 - x_3$, etc. Using these, the line scan transform is then defined as

$$G_{l \cap S}(\xi) = \sum_{k=2}^{2n} \sum_{i=1}^{k-1} (-1)^{i+k+1} \mathrm{I}\{x_k - x_i > \xi\}$$

for all interval lengths $\xi > 0$, and where

$$\mathrm{I}\{x_k - x_i > \xi\} = \begin{cases} 1, x_k - x_i > \xi \\ 0, otherwise \end{cases}.$$

The novelty of G becomes obvious only after close inspection. If $x_k - x_i$ represents an interval strictly interior or exterior to an object, the sum is incremented. On the other hand, if $x_k - x_i$ represents a collection of intervals that are both interior *and* exterior, the sum is decremented.

2.2 The Shape Descriptor

The shape descriptor, δ, of a set of objects is the average of the line scan transform of each randomly thrown member line l of the set of lines L

$$\delta_S(\xi) = \tfrac{1}{N} \sum_{L} G_{l \cap S}(\xi),$$

where N is the number of lines in L. $\delta_S(\xi)$ is unique [10] for any S as $N \to \infty$. It is possible, though not common, for $\delta_S(\xi)$ to be negative for certain values of ξ. It is worth noting that the value of $\delta_S(0)$ is the average number of objects in the set. The shape descriptor has some rare exceptions [11]. There are two known convex polygons with the same chord distribution and thus the same line scan distribution. Occurrences of this type seem to be extremely rare [12,13].

2.3 The Shape Metric

The shape metric μ for two object sets S and T is defined as

$$\mu(S,T) = \int_0^\infty \left| \delta_S(\ell) - \delta_T(\ell) \right| d\ell .$$

The metric as shown here is not scale invariant, but can be made so using any of several common methods [14], depending on the application.

2.4 Method of Random Line Placement

We generate lines that randomly and uniformly cover a set of objects [15]. Care must be taken that the distribution of the set of lines is probabilistically invariant under rigid rotations and translations. The object of interest is encompassed by a circle in $\Re^2$ or sphere in $\Re^3$, and the sampling lines are constructed within the enclosure. The sampling lines can be generated within a unit circle or sphere then scaled to encompass the object. We generate a set U of uniformly distributed random numbers and draw samples from it such that $u_i \in U$. In two dimensions, we generate the midpoint $\mathbf{P_c}$ of a random line as shown in Figure 3,

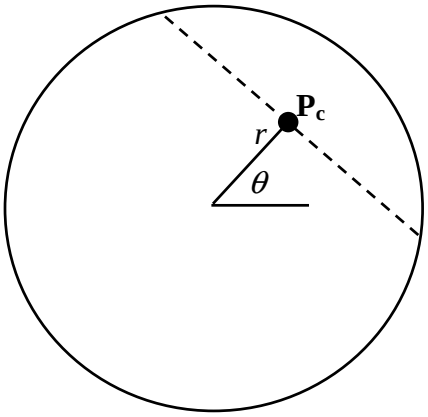

Figure 3. A random line is generated by determining its midpoint, $\mathbf{P_c}$, which is based on the randomly chosen r and θ.

where

$$r = u_1$$

and

$$\theta = 2\pi u_2 .$$

In three dimensions, we generate each of two endpoints on the surface of the sphere by generating coordinates such that

$$z = 1 - 2u_1$$
$$x = \cos(2\pi u_2)\sqrt{1 - z^2}$$
$$y = \sin(2\pi u_2)\sqrt{1 - z^2}.$$

In Figure 4 we illustrate a set of random lines in two dimensions that was generated in this manner.

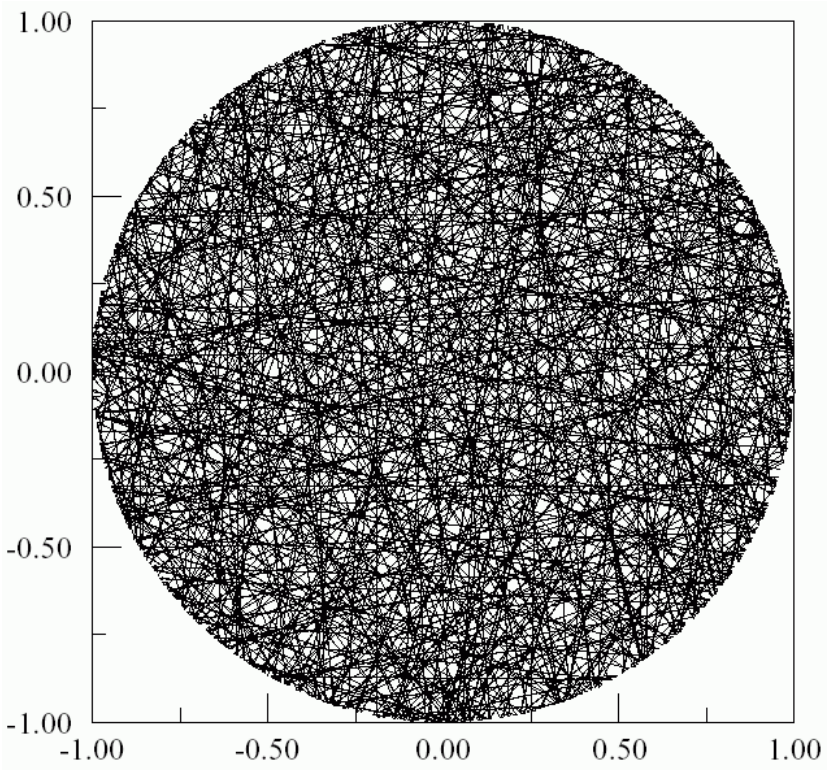

Figure 4. A set of randomly distributed lines on a circle.

3 Computational Considerations

The uniformly distributed points used in sampling are generated using Warnock's modification of Halton's quasi-random sequence [15]. A quasi-random sequence ω has the advantage of generating lines that approach a uniform distribution more quickly than would be the case using randomly generated points. The same set of lines is used for all objects so as to make comparisons more meaningful [16].

The $\omega_P(N)$ sequences are defined for each natural number N and each prime P by the following procedure.

1. Write the number N in base P: $N = \sum_0^\infty a_j P^j$ where only a finite number of the a_j are non-zero.
2. Modify the a_j by multiplying by a number S_P and reducing the result modulo P: $b_j = S_P a_j \bmod(P)$.
3. Accumulate the resulting number with the new digits reversed: $\omega_P(N) = \sum_0^\infty b_j P^{-j-1}$.

For the examples presented in this paper, the sequences used are based on the primes 3, 5, 7, and 11 with associated modifiers S of 2, 2, 5, and 3 respectively. For example, the 14th line in two dimensions would use $\omega_3(14)$ and $\omega_5(14)$ which can be computed as follows:

$14 = 2*3^0 + 1*3^1 + 1*3^2$ which is transformed into $\omega_3(14) = 1*3^{-1} + 2*3^{-2} + 2*3^{-3} = \frac{17}{27}$

and $14 = 4*5^0 + 2*5^1$ which becomes $\omega_5(14) = 3*5^{-1} + 4*5^{-2} = \frac{19}{27}$.

The actual computation of the line scan $G_{l\cap S}(\xi)$ can be done as follows. The ordered points of intersection , $(x_1, x_2, x_3, ..., x_{2n})$, give rise to $n(2n-1)$ segments. Each segment contributes to a histogram by scoring +1 if the subscripts of the endpoints of the segment have different parity and -1 if the parity is the same. This process is repeated over all the lines in the sample.

After all segments of all the sampling lines have been added to the histogram, a running total of the histogram is made starting with the longest length. If the histogram has m elements, then h_{m+1} is set to zero and the histogram is modified by $h_i = h_i + h_{i+1}$ with i running from m to zero. This use of the associative law allows each segment to be scored without scanning the segments individually along their length. The algorithm is equivalent to treating the indicator function , $\mathrm{I}\{x_k - x_i > \xi\} = \{^{1, x_k - x_i > \xi}_{0, otherwise}$, as a Heaviside function; adding its derivative to the histogram; then integrating the result.

4 Examples

4.1 A Three-Dimensional Sphere and Cube

In Figure 5, we show a set of two objects in $\Re^3$. The set consists of a sphere of diameter 2 centered at the origin with a smaller cube of edge size 0.5, internal and later external to the

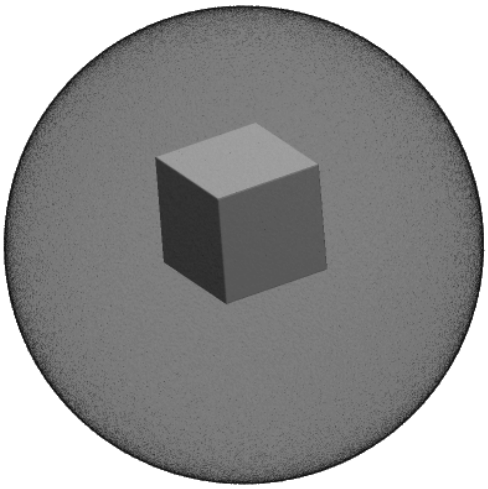

Figure 5. A cube of edge length .5 enclosed in a sphere of diameter 2. Both objects are solid.

sphere, all defined analytically. In Figure 6 we initially show the descriptors of the sphere and cube separately. The next two descriptors represent the cube internal to the sphere, first centered on the origin, then shifted along one axis. The last two descriptors represent the cube emerging from and external to the sphere.

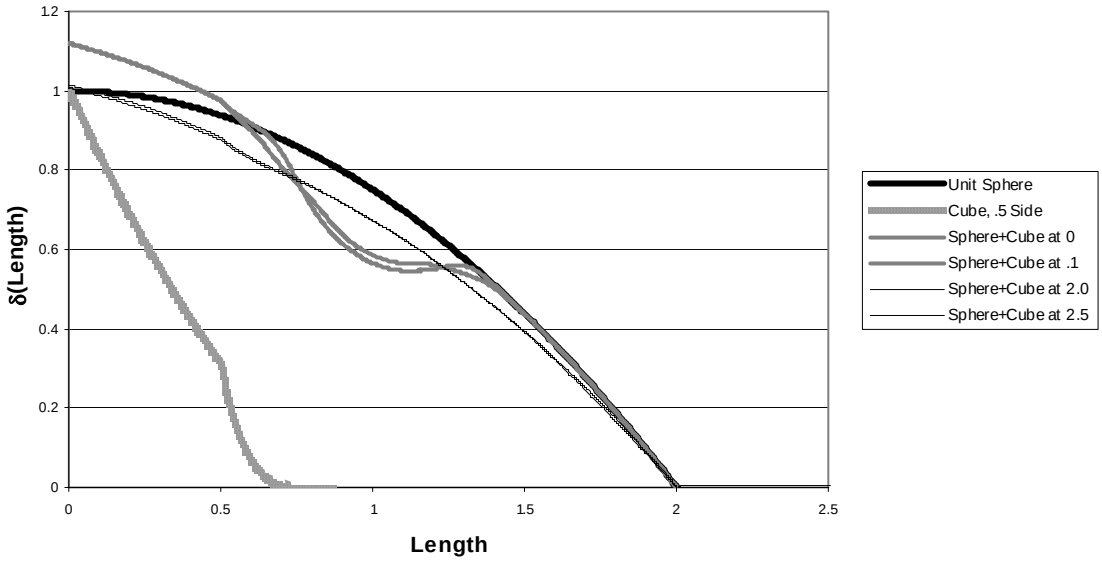

Figure 6. The 3-D shape descriptors for a sphere and a cube. For the two cases in which the cube is contained within the sphere, the resulting shape descriptor is approximately that of the sphere minus that of the cube. On the other hand, when the cube is emerging or external to the sphere, the descriptor is dominated by the size of the sphere and the distances between it and the cube. Not visible on the plot are small but non-zero values near lengths of 2.5.

4.2 A Sphere Morphing to an Ellipse

We will use the six objects in Figure 7 to illustrate the shape descriptor and metric. The first is a perfect circle, the others represent an elongation in the vertical axis of the circle in

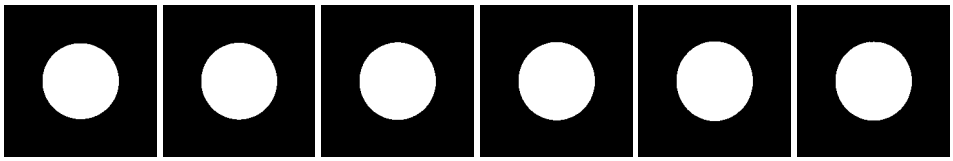

Figure 7. The left-most object is a perfect circle of diameter .5. Proceeding to the right, the objects have an elongation in the vertical axis in increments of 1%.

increments of one percent, a change possibly unnoticed by the unalerted eye. As the vertical axis lengthens, we would expect to see longer lengths appear in the corresponding shape descriptor, as indeed we do in Figure 8.

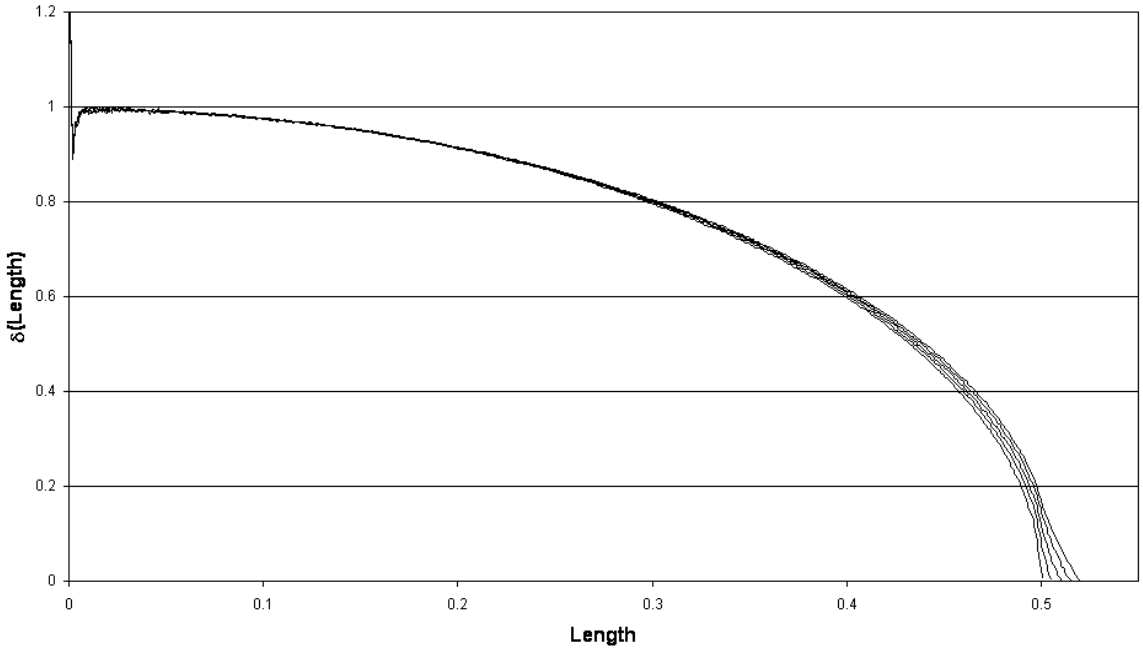

Figure 8. The shape descriptors of the six objects in figure 7. Note the maximum length contained within the perfect circle is .5, its diameter. The descriptors of the other objects indicate the presence of longer lengths as the vertical axis of the circle is lengthened. (The large number of very short lengths indicated in each descriptor is the result of spatial quantization.)

The shape descriptors change in an interesting manner when the edges of the objects are perturbed by random noise, as we show in the case of the circle in Figure 9.

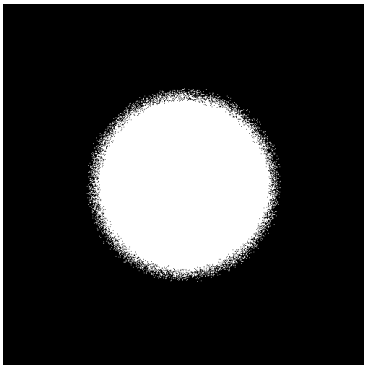

Figure 9 The circle perturbed by random noise. The diameter remains .5, but the image has been magnified to show the edge effects more clearly. The remaining objects in figure 7 were perturbed in a similar manner.

As shown in Figure 10, the shape descriptors for the corresponding objects are different in three ways. First, the descriptors indicate the presence of longer lengths resulting from the

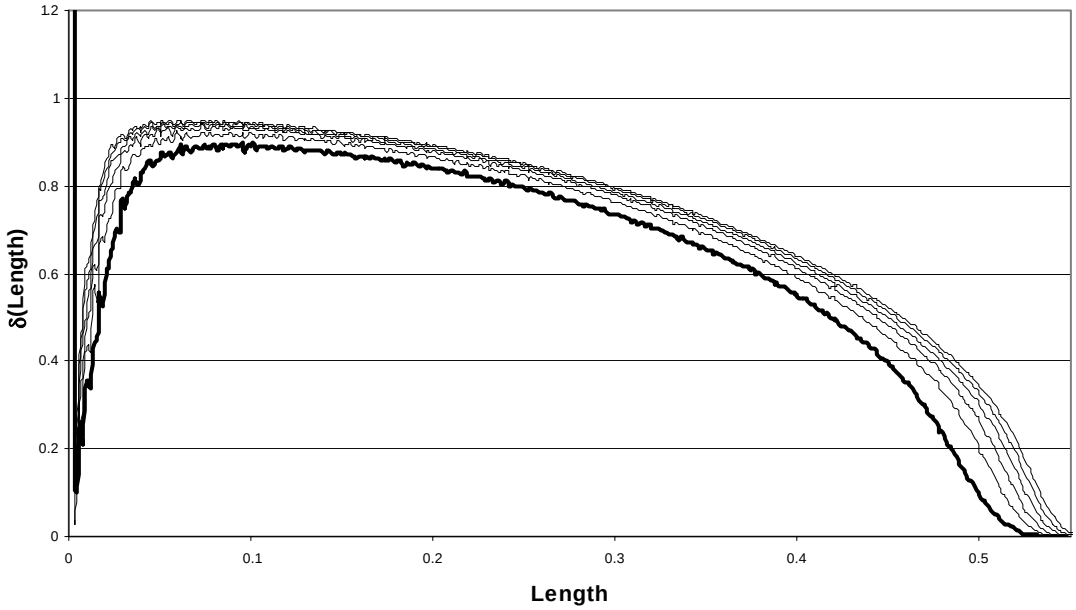

Figure 10. The shape descriptors for the objects in Figure 7 after the edges are perturbed by random noise. The descriptor of the perfect circle of radius .5 is drawn in the heavier line.

addition of the noise. Second, the number of very short lengths, lengths close to the added random noise, is increased greatly. Third, and least expected, is the decreased value of each descriptor at lengths around .02. We speculate that this is caused by the introduction of many short intervals that lie internal and external to the noise in the edge regions.

The metric used to compare the shape of two objects is obtained by calculating the absolute difference in the corresponding shape descriptors. In Figure 11 we show the metrics for each object in Figure 7 compared with the perfect circle as well as the metrics for the noisy objects compared to the noisy circle.

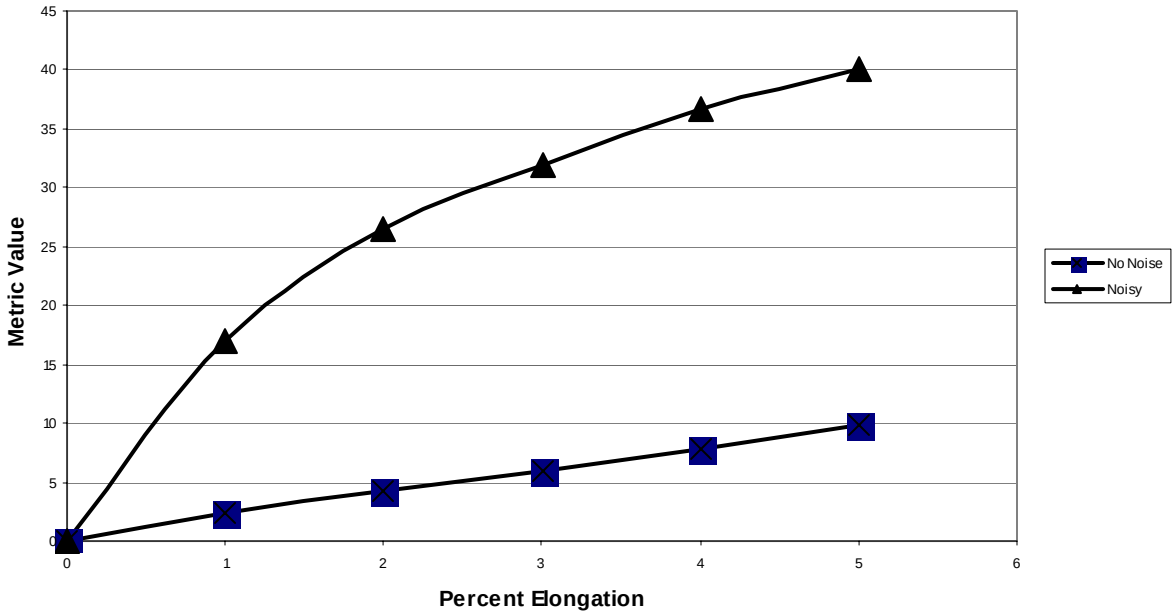

Figure 11. We plot metrics for the noisy and clean objects. Note that the difference between the noisy circle and itself as well as the clean circle and itself is zero.

4.2 Shock-Induced Instabilities

In Figure 12 we show several examples of three gas columns that have been impacted by a Mach 1.2 planar shock front [17]. We have learned experimentally that the gas will assume one of the four morphologies depicted in Figure 12

.

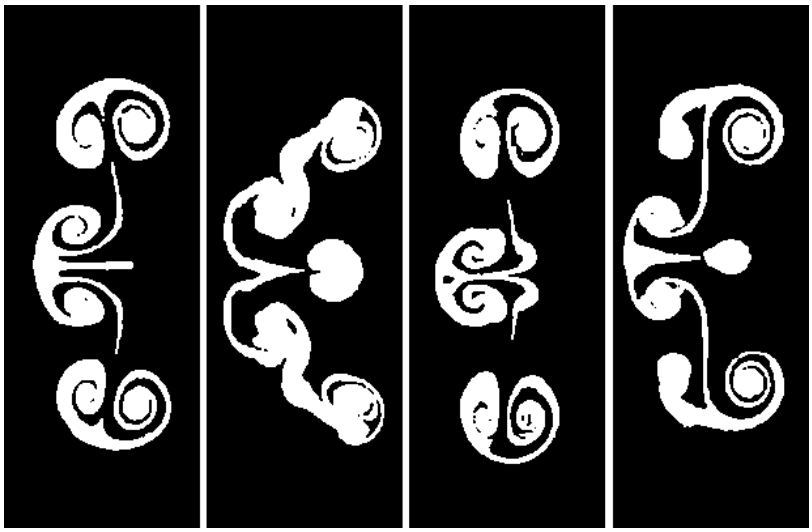

Figure 12. We depict the four morphologies assumed by three gas columns after being impacted with a Mach 1.2 planar shock front.

As a test of the shape metric, we first compute the line scan transforms of each of the four morphologies and plot them, as shown in Figure 13. We compute the metric of the similarity

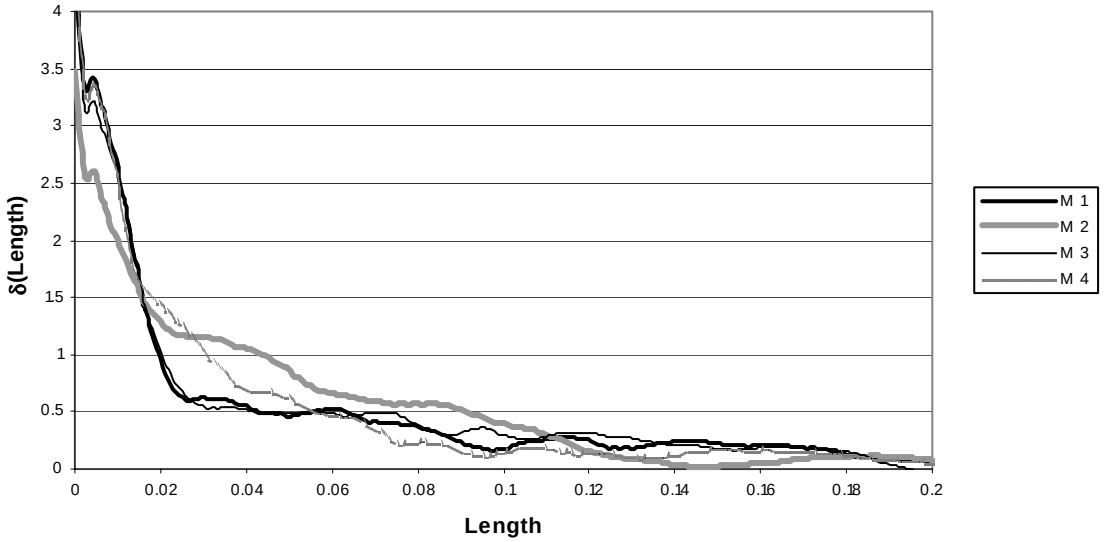

Figure 13. The line scan transforms of the four morphologies. Note that the value of $\delta_S(0)$ is approximately equal to the number of objects in each of the morphologies in Figure 12.

of each morphology to morphology One by computing the absolute difference between the line scan transform of morphology One and each of the transforms for the four morphologies. These values are plotted in Figure 14 and compared with values obtained from Hu moments. In this

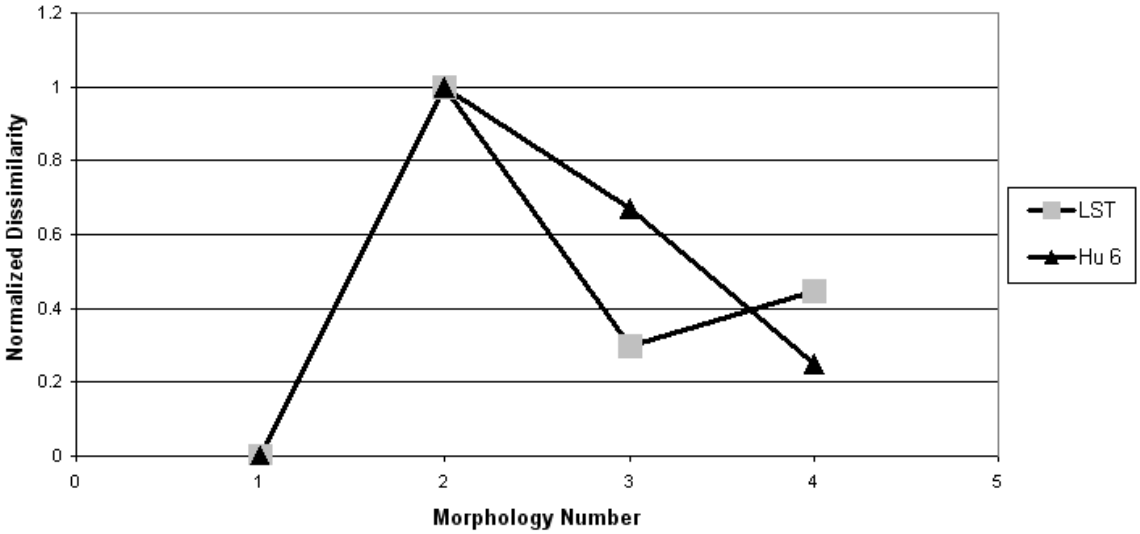

Figure 14. We compare the four morphologies in Figure 12 with Morphology One, the left-most. We use two comparison methods, the first based on the line scan transform, the second on Hu moments. The results are comparable, and both methods show Morphology Two as most different from One. The two methods differ on which morphology is closer to One, with the LST favoring Three and Hu moments Four.

particular example, the two methods differ on which morphology is closest to One, but they agree on Morphology Two being the least similar to One, a finding probably consistent with different human observers

5 Conclusion

We have presented a novel shape descriptor based on the line scan transform. Our initial experiments with it suggest that it performs in a logical and useful manner and may be useful in certain image analysis problems.

6 References

1. T. Pavlidis, "A Review of Algorithms for Shape Analysis," *Comput. Graphics Image Processing*, **7**, pp 243-258, 1978.
2. C. T. Zahn and R. Z. Roskies, "Fourier Descriptors for Plane Close Curves," *IEEE Trans. Comput.*,Vol C-21, No. 3, pp 269-281.
3. H. Freeman, "On the Encoding of Arbitrary Geometric Configurations," *IEEE Trans. Elec. Computers*, Vol EC-10, pp 260-268.
4. I.Young, J. Walker, and J. Bowie, "An Analysis Technique for Biological Shape," *Comput. Graphics Image Processing*, **25**, pp 357-370, 1974.
5. H. Blum, "Biological Shap and Visual Science Part 1," *J. Theoret. Biol.*, **38**, pp 205-287, 1973.
6. M. K. Hu, "Visual Pattern Recognition by Moment Invariants," *IRE Trans. Info. Theory*, IT-8, pp 179-187, 1962.
7. E. R. Dougherty, An Introduction to Morphological Image Processing, SPIE Optical Engineering Press, Donald C. O'Shea, Ed., 1992.
8. J. Cabo and A. J. Baddeley, "Line Transects, Covariance Functions, and Set Convergence," A*dv. Appl. Prob.*, **27**, pp 585-605, 1995.
9. R. Osada, "Shape Distributions," *ACM Transactions on Graphics*, Vol. 21(4), pp 807-832, 2002.
10. J. Cabo and A. J. Baddeley, "Line Transects, Covariance Functions, and Set Convergence," A*dv. Appl. Prob.*, No. 27, pp 585-605, 1995.
11. C. L. Mallows and J. M. Clark, "Linear-intercept distributions do not characterize plane sets", J. Appl. Prob. **7**, pp 240-244, 1970.
12. E. Green and P. Waksman, "Grid analysis: continuing the search for a metric of shape", J. Math. Psych. **31,** No. 4, pp 338-365, 1987.
13. P. Waksman, "Plane polygons and a conjecture of Blaschke's," Adv. In Appl. Probab. 17 No. 4, pp 774-793, 1985.
14. Sven Loncaric, "A Survey of Shape Analysis Techniques," *Pattern Recognition*, Vol. 31, No. 8, pp 983-1001.
15. T. Warnock, "Computational investigations of low-discrepancy point sets. II." In Niederreiter, Harald (ed.) et al., *Monte Carlo and quasi-Monte Carlo methods in scientific computing.* Proceedings of a conference at the University of Nevada, Las Vegas, Nevada, USA, June 23-25, 1994. Berlin: Springer-Verlag. Lect. Notes Stat., Springer-Verlag. 106, pp 354-361, 1995.
16. X. Li,; W. P. Wang; Martin, RR; Bowyer, A. "Using low-discrepancy sequences and the Crofton formula to compute surface areas of geometric models." *Computer-Aided Design*, 35, pp 771-782, 2003.
17. S. Kumar, et.al., "Complex flow morphologies in shock-accelerated flows" , Los Alamos National Laboratory, in preparation.